



The Effect of Triangle Slope Variation on Froude Number with Numerical Simulation

Mukhsan Putra Hatta ^{1*}, Ira Widyastuti ², Andi Muh. M. Makkarumpa ²

¹ Department of Civil Engineering, Faculty of Engineering, Hasanuddin University, Gowa 90235, Indonesia.

² Department of Civil Engineering, Faculty of Engineering, Cenderawasih University, Papua 99332, Indonesia.

Received 21 August 2023; Revised 11 November 2023; Accepted 19 November 2023; Published 01 December 2023

Abstract

Many parameters can be influenced by speed flow, like form resistance and speed flow. Form obstacles influence structure turbulent flowing water, so that can raise potency change speed and pattern flow around the structure building. This study considers the tilted corner prisoner structure triangle and incoming water flow to influence the pattern and speed flow that occur after the genre through the obstacle triangle using IRic simulation. IRIC is a simulation platform that supports numeric and various breaker computing problems in water science and engineering. The variations of the corner prisoner plate triangle used in this study are 30°, 45°, and 60°. The transverse channel is blocked with a ratio of $\beta = 1/10$, and upstream-downstream boundary conditions are open. Results show what will happen in the genre critical moment pass structure. Because the change is significant, Froude's number. Observations that took place showed that speed flow on each slope was stable before the pass structure and was not stable after the pass structure. Whirlpools occur on a 45° slope, so the speed flow that occurs will increase significantly. On an incline of 60°, it will have the largest Froude number, which is caused by the depth (D) created by the 60° angle being higher in comparison with another slope. For an incline of 30°, show speed, more flow, and a constant flow with a bigger Froude number.

Keywords: Triangular Obstacles; Froude's Number; Slope; Flow Speed.

1. Introduction

Well-known research topics primarily focus on hydraulics and river engineering, specifically aimed at simulating water flow in rivers. Pattern changes can occur in the channel due to the presence of buildings and other structures, potentially resulting in a change in speed around these structures. One alternative method for dampening energy that travels along the channel is the use of a dam with channel obstruction. The influence of structural turbulence affects the flow of water. This is because the current turbulent behavior deposits turbidity as suspension sediment [1]. Moreover, since the flow is separated by a non-movable barrier (such as buildings) placed on the base of the river, the flow speed increases and influences the sediment base from the acceleration and deceleration of flow around the barrier. The placement of an obstacle at the base of the channel influences the change in speed (friction, u^*), which is then compared backward to maintain the integration (C). The speed value swipe (u^*) will increase to match the speed swipe under normal conditions (u^*_L), causing the flow rate to slow down in the area upstream of the obstacle. This is because the obstacle impedes the flow rate, requiring more energy for the flow to return to its normal state [2].

Previous studies have focused on analyzing flow stability through obstacles and flow speed [3-7]. These studies have identified ways to mitigate the risk of dam failure by accurately estimating the effective parameters concerning energy

* Corresponding author: mukhsan.hatta@unhas.ac.id



<http://dx.doi.org/10.28991/CEJ-2023-09-12-012>



© 2023 by the authors. Licensee C.E.J, Tehran, Iran. This article is an open access article distributed under the terms and conditions of the Creative Commons Attribution (CC-BY) license (<http://creativecommons.org/licenses/by/4.0/>).

dissipation, dam collapse, and flooding direction around both natural and artificial obstacles downstream [3]. Additionally, Yaghoubi et al. (2017) demonstrated that an area with negligible speed growth and increasing real concentration upstream around every obstacle becomes larger [5]. An experimental and numerical study was conducted on obstacles placed at the bottom of a channel, where a vortex shedder (a common component of a vortex flow meter) is situated on the same side as the structure flow around a cylinder triangle. Flow characteristics such as contour vortices, current line cross-section patterns, vector speed, field speed, Reynolds stress correlation, Strouhal number, and drag coefficient were examined using Particle Image Velocimetry (PIV) techniques and the Large Eddy Simulation (*LES*) turbulence model [4]. The study also utilized the *RANS* (Reynolds Averaged Navier-Stokes) type of turbulence model, which is widely used in practical applications [8]. However, due to its impact, it requires more *CPU* and memory time compared to *LES* and *DNS*. Despite these potential drawbacks, the advantages, limitations, and areas for improvement of the *RANS* model are still worth considering. To address the Reynolds stress term in the mean Navier-Stokes equation, the *k-ε* model is commonly used [8, 9]. This research further explores the phenomenon of flow patterns spilling vortex behind triangle barriers, showing significant changes with the *Reynolds* number [10]. The approach suggests that flow phenomena slow down before passing the obstacle but experience no change in speed after passing the obstacle, especially when the obstacle is placed in a submerged condition at the bottom of the channel. The ultimate goal of this research is to review the variation of obstacle effects in flow damping using the simulation *iRic-Nays2DH*, with the damping effect varying based on the Froude number.

2. Basic Equations of the Model

2.1. Equality Conservation of Fluid Mass

As established in previous studies, the principle of eternal fluid mass dictates that the incoming fluid mass is equivalent to the outgoing mass. This principle forms the basis for writing the mass balance equation for fluid particles. The equation considers the rate of mass particle flow and the clean mass rate in the fluid element.

The rate of mass particle flow can be represented as follows:

$$\frac{\partial \rho}{\partial t} (\delta x \delta y \delta z) \quad (1)$$

where, ρ is mass type (kg/m^3); t is time (s) and $(\delta x \delta y \delta z)$ element volume fluid (m^3).

Additionally, we delineate a flow passing through a fluid element on a plane using three dimensions, as depicted in Figures 1 and 2.

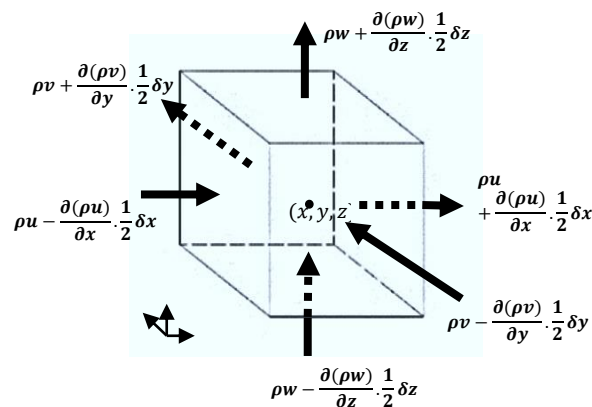


Figure 1. Direction of mass flow in fluid elements

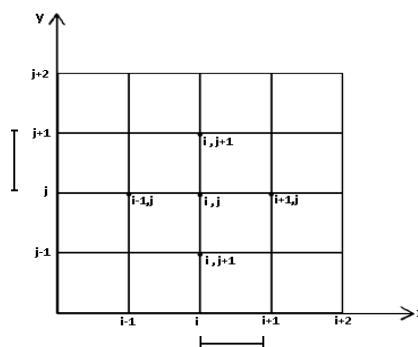


Figure 2. Grid points count on x and y

Equation 2 represents the fluid rate continuity equation, which is expressed in (kg/s). Given that the volume of the fluid particle element remains constant, it can be formulated as follows:

$$\frac{\partial \rho}{\partial t} + \frac{\partial(\rho u)}{\partial x} + \frac{\partial(\rho v)}{\partial y} + \frac{\partial(\rho w)}{\partial z} = 0 \quad (2)$$

Equation 2 above is an equation for the continuity of fluid flow that is not permanent (*unsteady*) in three dimensions. Meanwhile, if it is reviewed in two dimensions, the equation is as follows:

$$\frac{\partial \rho}{\partial t} + \frac{\partial(\rho u)}{\partial x} + \frac{\partial(\rho v)}{\partial y} = 0 \quad (3)$$

2.2. Fluid Momentum Equation

According to Newton's second law, the change in momentum of a fluid particle is equal to the sum of the forces acting on the particle. The change in fluid momentum in the x and y directions is as follows:

$$\text{x-direction: } \frac{\partial(\rho u)}{\partial t} + \frac{\partial \rho u^2}{\partial x} + \frac{\partial(\rho uv)}{\partial y} \quad (4-a)$$

$$\text{y-direction: } \frac{\partial(\rho v)}{\partial t} + \frac{\partial \rho uv}{\partial x} + \frac{\partial(\rho v^2)}{\partial y} \quad (4-b)$$

Equations 4-a and 4-b represent the equations of change in momentum, where the product of mass speed (kg/s) and velocity (m/s) is considered. According to the Nays2DH solver manual (2014) [11], the motion of the flow is divided into two coordinate systems. One is the orthogonal system (x, y), and the other is the linear curve or moving boundary fitted coordinates (MBFC) system.

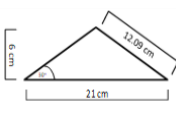
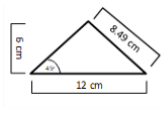
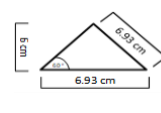
3. Materials and Method

3.1. Determination of Geometry

The Nays2DH is a computational model designed to simulate two-dimensional (2D) horizontal flow. It accounts for any obstacles within the calculation target area, which is determined based on cell calculations. There are various arrangements available for defining the end boundary conditions upstream and downstream. These include periodic boundary conditions, setting elevation at the end face downstream, and speed at the end upstream. This flexibility makes it easier to set boundary conditions based on observational data. For each cell calculation, an object can be defined to identify obstacles.

In the simulation study, we used a specific geometry for the channel. The channel is 6 meters long, 40 cm wide, and 50 cm high. An obstacle, in the form of a triangle, is placed in the middle section of the channel, 3.00 meters away from the upstream channel, with a slope of 0.001 (see Table 1).

Table 1. Model design

Open Channel (cm)	Triangle Model (cm)		Shape
Square	Slope (tan Θ)	30°	
	L	40	
	h	6	
	P	21	
	Slope (tan Θ)	45°	
	L	40	
	h	6	
	P	12	
	Slope (tan Θ)	60°	
	L	40	
	h	6	
	P	6.9	

3.2. Outcome Simulated Network

The simulation integrates *Nays2D* and *Morpho2D* to provide an accurate flow simulation. It uses regular software capabilities to simulate changes in flow patterns within channels and various obstacles within the target area, based on cell-based calculations. For each *cell* calculation, an object is determined to identify obstacles. As a result, a channel with a hydraulic structure can be combined into a single downstream channel. The steps used for combining are accommodated by the application for determining Type A mergers: *branch junctions* or Type B: *T Junction*.

4. Result and Discussion

4.1. Configuration System

The flow design assumes two-dimensional U_x and U_y , with isothermal and kinetic flow constants. The relevant equations, which are derived from Equations 3 and 4, describe the intended kinetic flow, which is measured by the Froude number. The Froude number is a non-dimensional parameter that indicates the relative effect of inertia to gravity. It measures the resistance from a moving object through the water and compares objects of different sizes based on speed or different distances [12]. The formula for Froude's number is $F_{loc} = \frac{U_{max}}{\sqrt{g D \cos \theta}}$, where U is the maximum flow speed, g is the acceleration due to gravity, D is the diameter of the pipe, and θ is the angle between the pipe diameter and the flow direction. Figure 3 shows a schematic cross-section of the channel, with a triangle obstacle placed in the middle of the channel. The transverse cross-section of the channel shows a straight, upright direction of flow with a tall channel (H), length of the channel (L), and inflow length (l). During the simulation, the area is divided into 600 grid points in the x direction (N_x) and 43 points in the y direction (N_y). The flow limit conditions are free and uniform, and the roughness base uses the Manning method. The upstream condition is open. The parameter values can be seen in Table 2 and Figure 4. The model cross-section of 3D channels and obstacles has been presented in Figure 5.

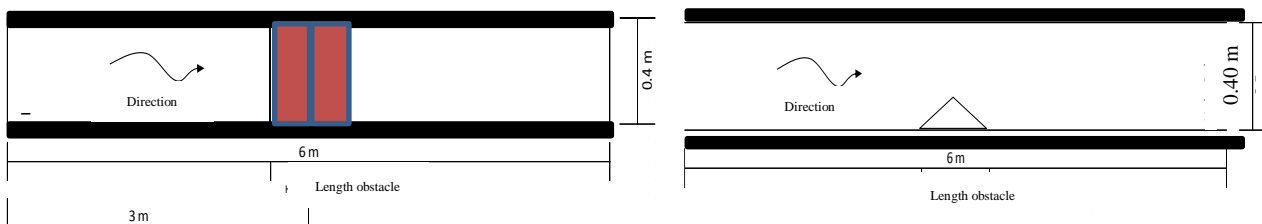


Figure 3. Schematic cross- section channels and barriers

Table 2. Simulation Design

Parameter	Notation	Value
Number of grids on x	N_x	601
number of grids on y	N_y	43
input Discharged	Q	0,01
Manning Coefficient	n	0.01
Block Ratio	$\beta = d/H$	0,10

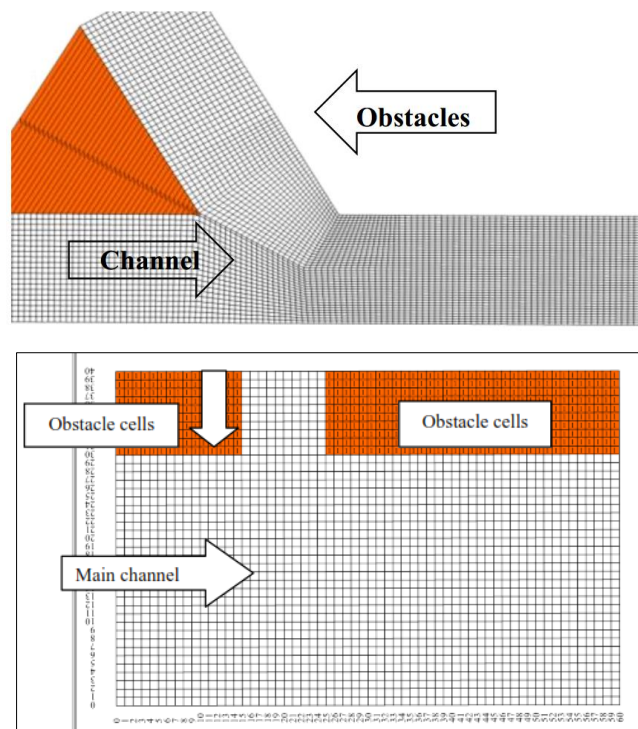


Figure 4. Schematic concept of the grid on the (a) Type A and (b) Type B grids

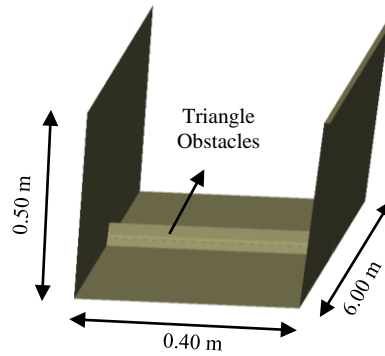


Figure 5. Model cross-section 3D channels and obstacles

Figure 6 shows the flowchart of the research methodology through which the objectives of this study were achieved.

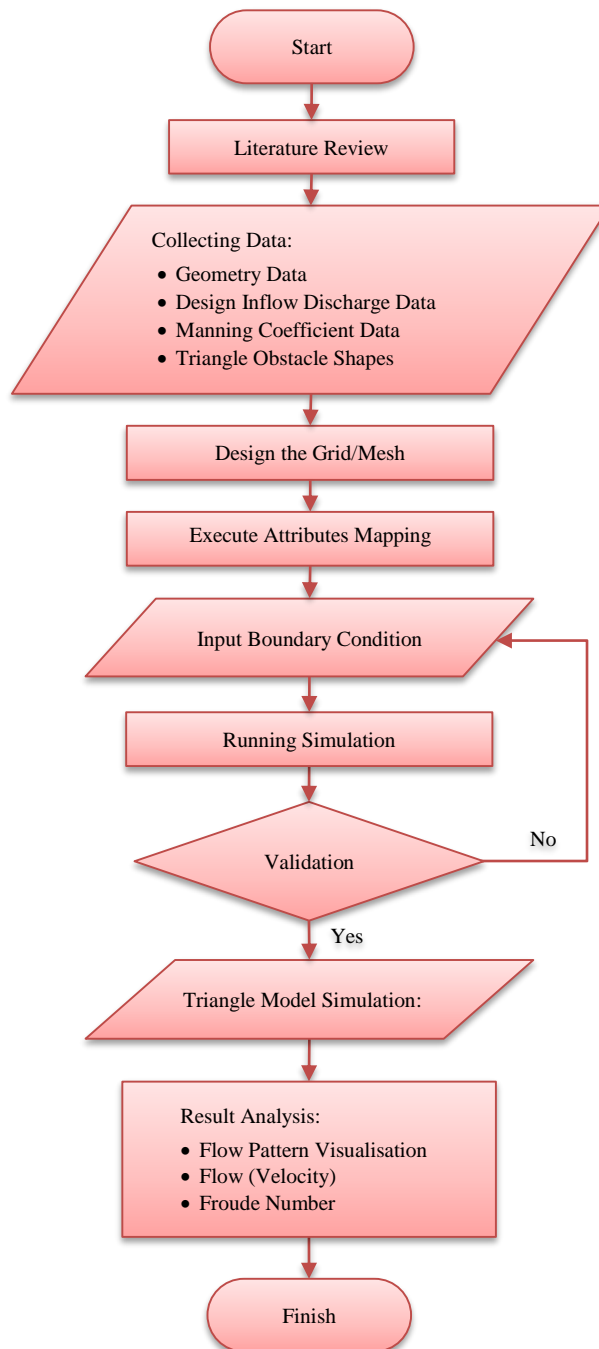


Figure 6. Flowchart of the research methodology

The geometry scheme for 2D channels and barriers triangle has been presented in Figure 7.

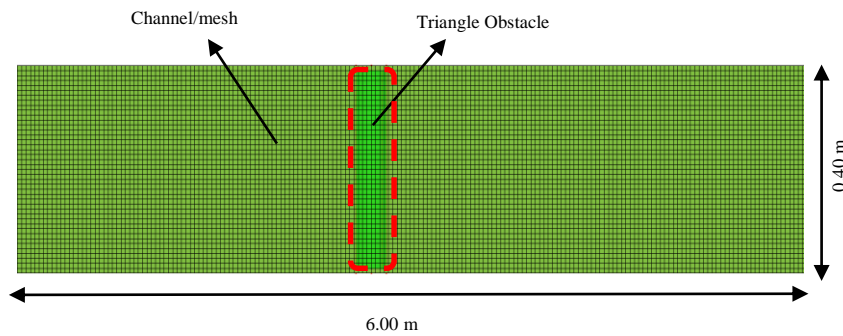
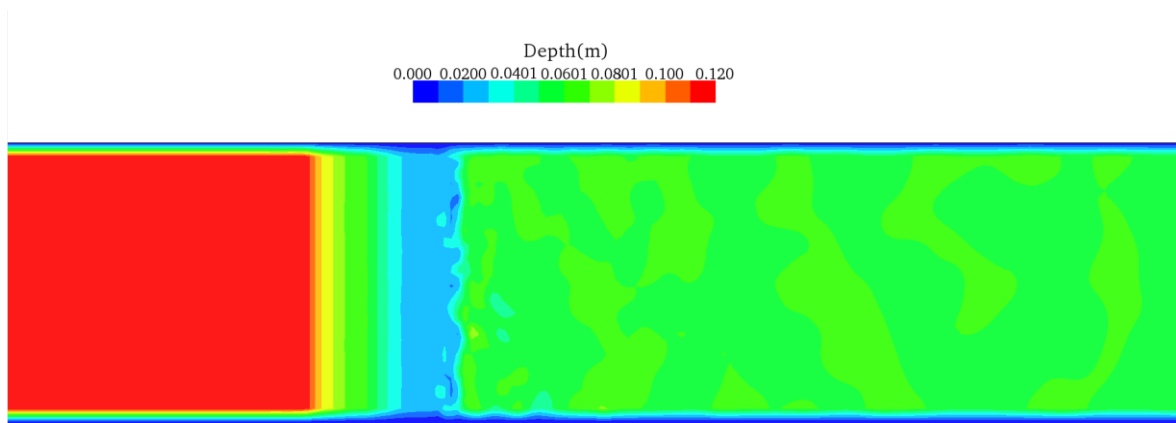
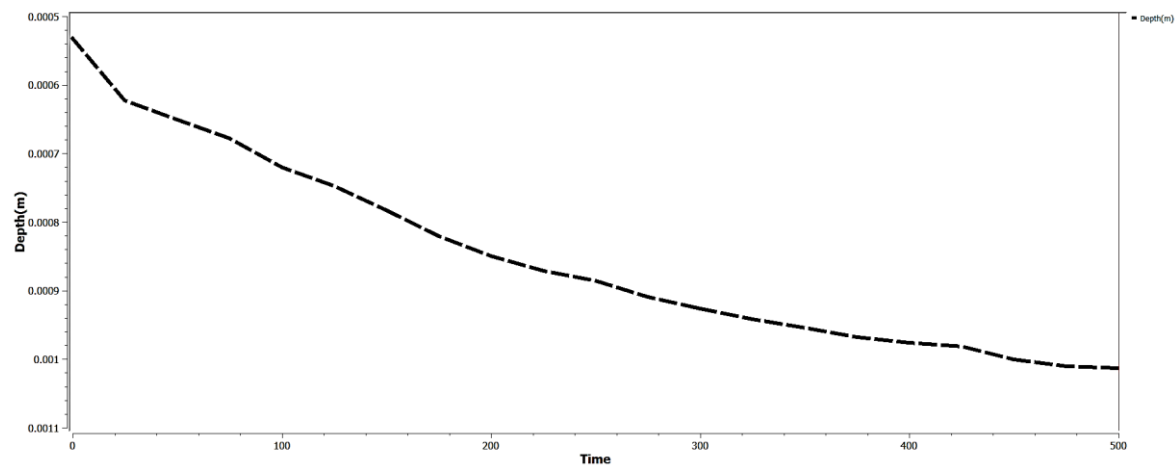


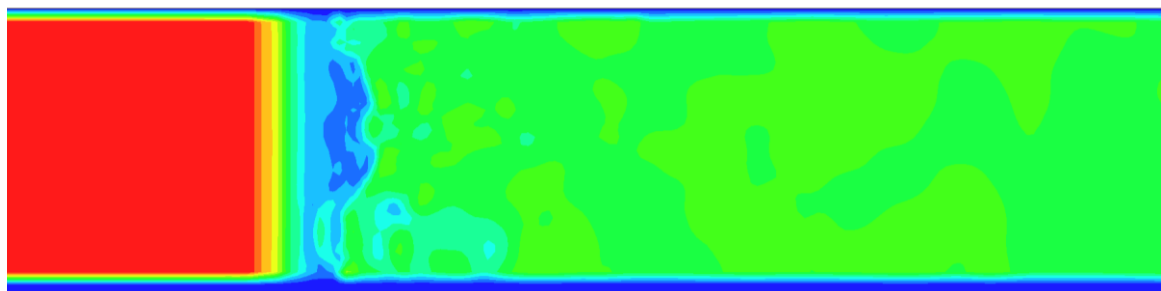
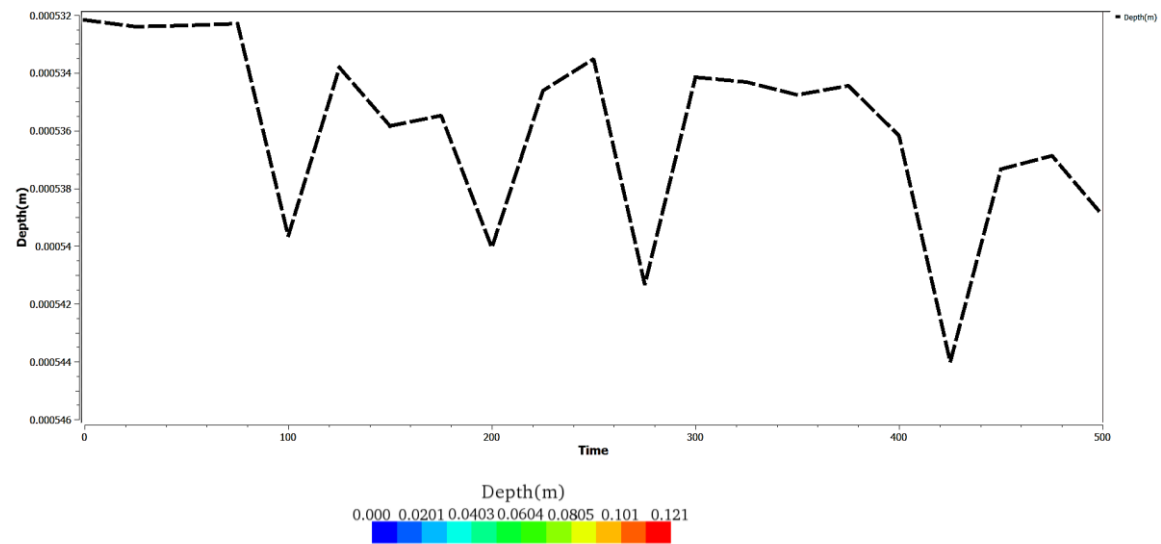
Figure 7. Geometry scheme for 2D channels and barriers triangle

4.2. Simulation Result

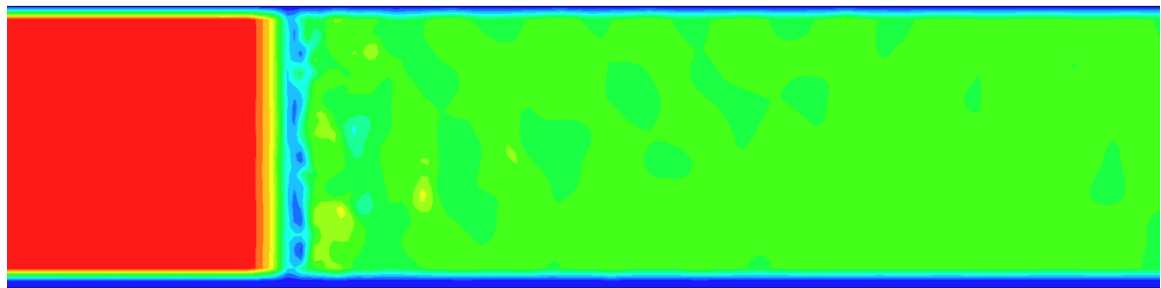
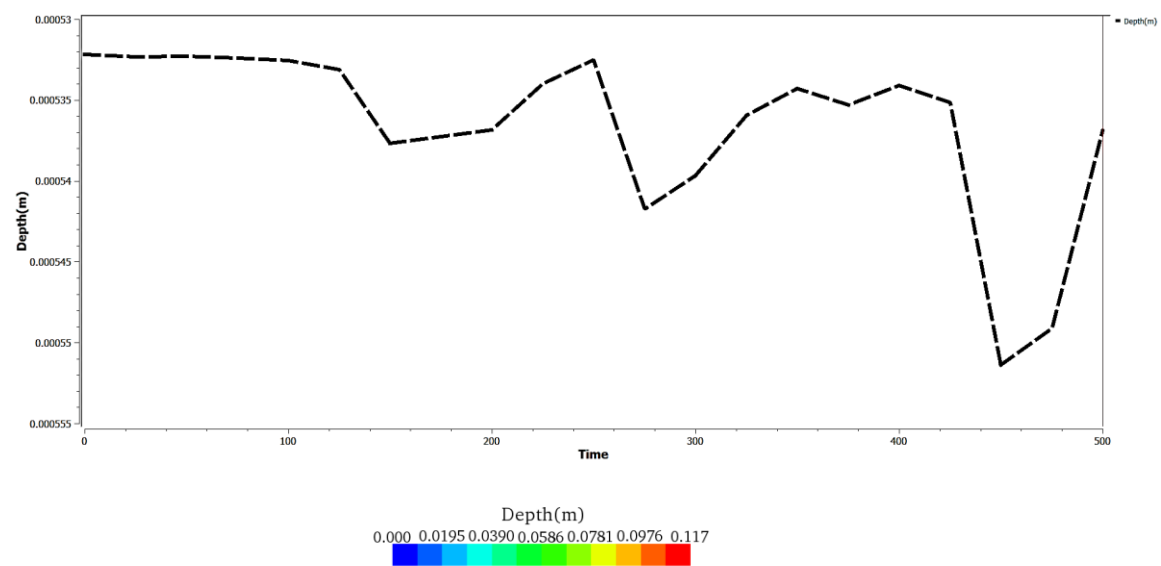
The simulation results indicate that the flow around all obstacles is modeled based on Nx/Mrs , with the ratio of the height of the water level (h_o) to the height of the channel being $\beta = 1/10$. A tall obstacle of 6.00 cm is used, with variations in slopes of 30° , 45° , and 60° (Figure 5). The analysis of the flow pattern reveals that the upstream area experiences an increase in water surface level and then encounters resistance (downstream), leading to a decrease in water level. In the downstream area, the flow tends to stabilize at a 30° inclination, but instability occurs at slopes of 45° and 60° (Figure 8). Observations (Figure 9) show that the flow pattern immediately past the obstacle causes a relative reduction in flow speed. However, fluctuations occur due to the release of eddies in the downstream area of the triangle, with conditions taking place along its channel (downstream). From the three obstacle triangles, the largest velocity flow and fluctuations occur in the 45° slope model (M_2). However, the velocity is the smallest relative average after passing the obstacles.



$M_1=30^\circ$



$M_2=45^\circ$



$M_3=60^\circ$

Figure 8. Flow pattern speed and connection depth (D) vs Time (T)

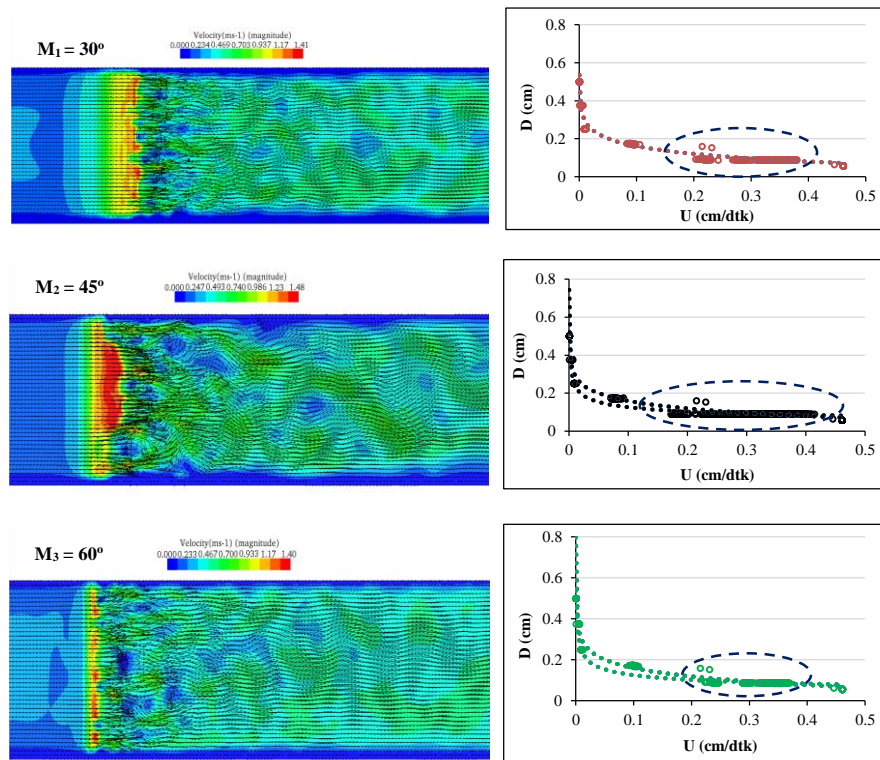
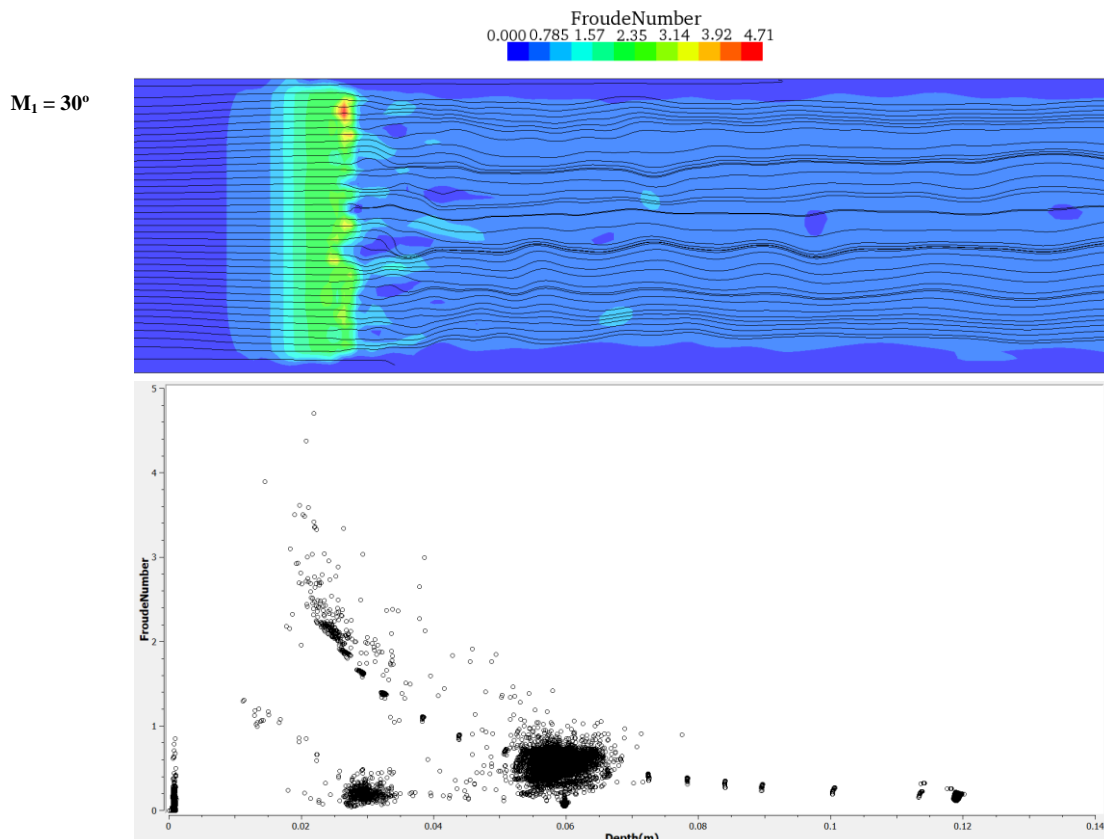
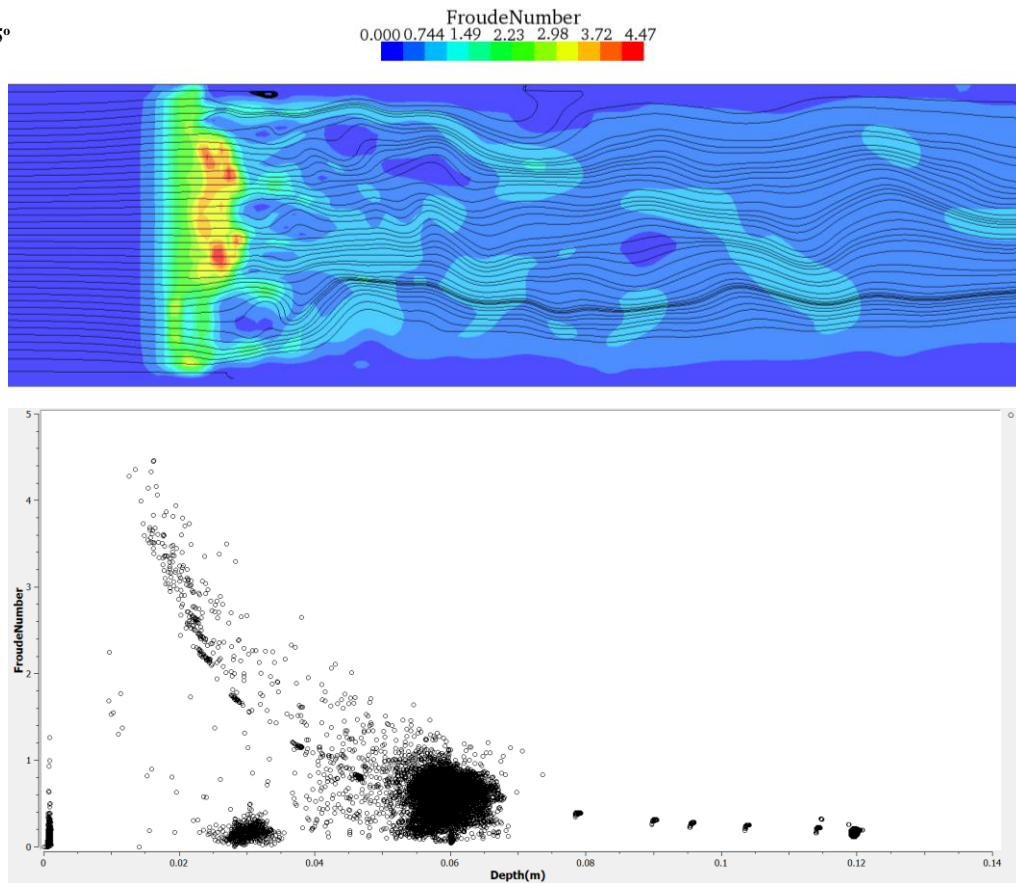


Figure 9. Flow pattern speed and connection depth (D) vs speed (U)

The *Froude* number on channels is significantly influenced by the flow speed. The *Froude* number is compared directly with the flow speed. In the simulation, the dimensions of the channel used remain the same, as the *Froude* number varies differently for each triangular plate shape being simulated. All triangular plates have a *Froude* number greater than 1. The maximum *Froude* number is achieved at an angle of 30° , reaching a value of 2.67, which corresponds to a supercritical flow type. However, after the triangular plate, the *Froude* number decreases significantly until it reaches a value less than 1, indicating a subcritical flow type. Each triangular plate differs in this regard. When marking the *Froude* number at 60° , the results show a smaller *Froude* number, even less than 1, at all distances. Thus, it can be concluded that at a 60° angle, the flow type is subcritical (see Figures 10 and 11).



$M_2 = 45^\circ$



$M_3 = 60^\circ$

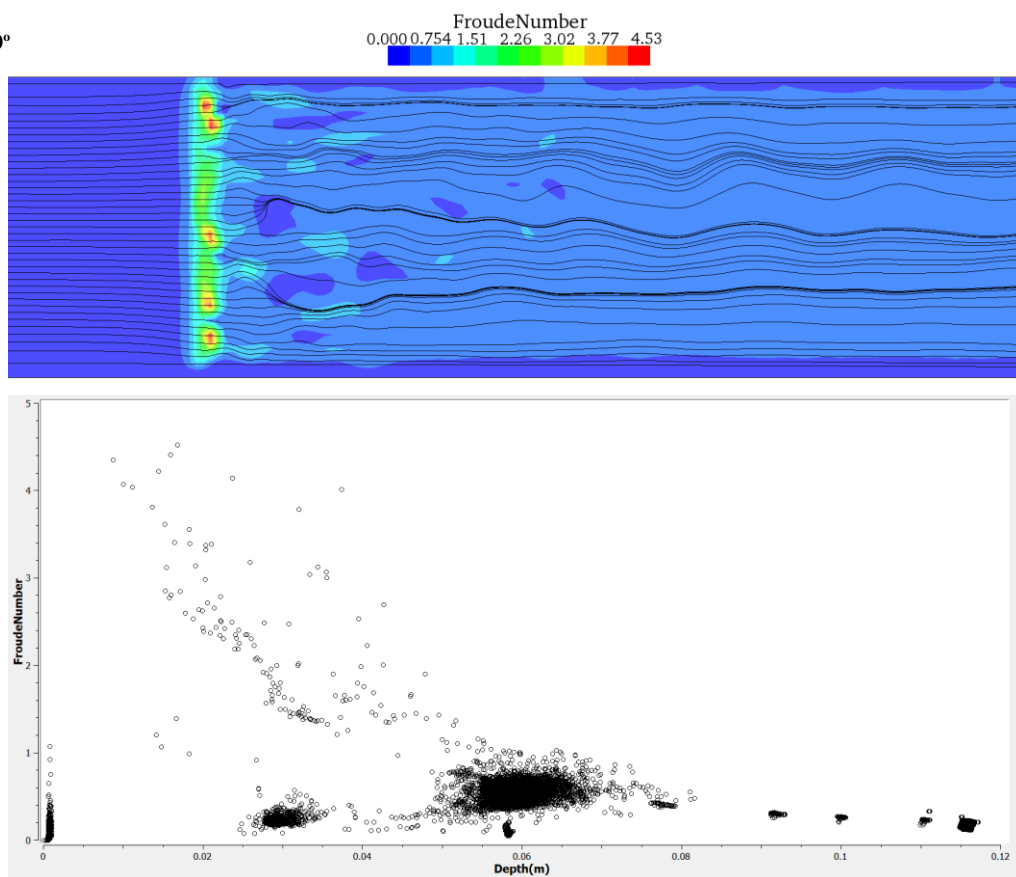


Figure 10. Flow pattern based on connection Depth (D) vs Froude (Fr)

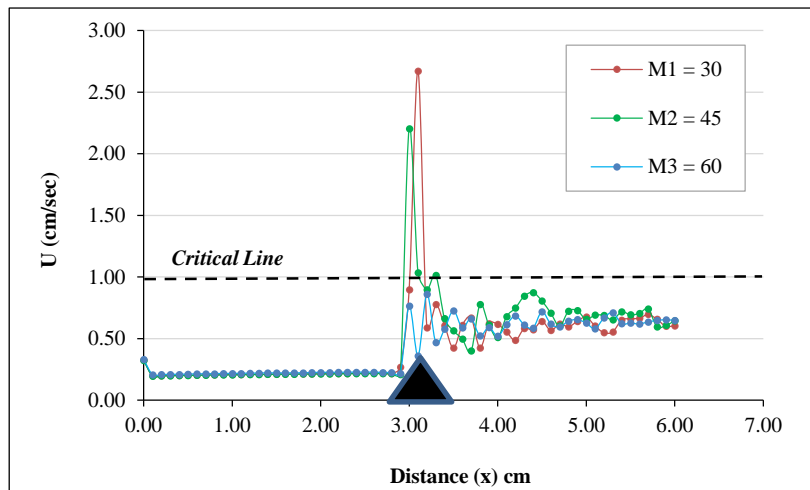


Figure 11. Profile elongated Froude Number (Fr)

4.3. Validation of The Simulation Result

In validating the simulation results, computations were performed using the *i-Ric Nays2DH* reference for validation. This is an empirical calculation based on the average flow rate in an open channel, a calculation that had been conducted by researchers in the past [13]. A triangular structure with a 30° incline was used in the simulation. Figure 12 illustrates the similarity between the simulation results and the experimental results.

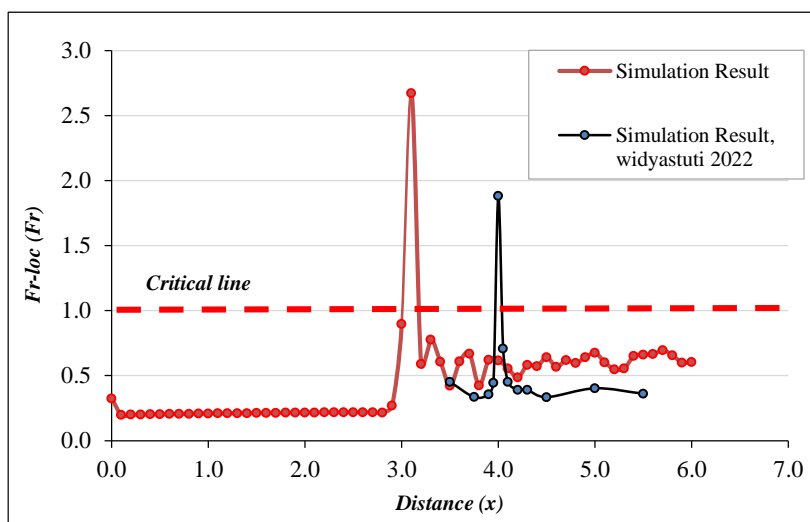


Figure 12. Profile elongated Froude Number (Fr)

5. Conclusion

The study demonstrates that the *Nays-2DH* simulation produces reliable results for examining the flow of fluid around structures. The results indicate that the critical moment of flow passing through an obstacle is marked by a significant change in Froude's number. Observations taken during the simulation show a steady flow before the structure and increased turbulence afterward. Furthermore, the slope with maximum velocity and the greatest Froude number is at a 45° incline. The largest vortex occurs at a 45° slope, causing a significant increase in flow velocity. The highest Froude number occurs at a 60° slope, which is attributed to the higher depth (*D*) created by the 60° angle compared to other slopes. For a 30° incline, the flow speed is more consistent, with a larger Froude number.

6. Declarations

6.1. Author Contributions

Conceptualization, M.P.H. and I.W.; methodology, I.W.; software, I.W. and A.M.M.; validation, M.P.H.; formal analysis, I.W. and A.M.M.; investigation, I.W. and A.M.M.; resources, I.W. and A.M.M.; data curation, I.W.; writing—original draft preparation, I.W.; writing—review and editing, M.P.H.; visualization, I.W.; supervision, M.P.H.; project administration, M.P.H.; funding acquisition, I.W. All authors have read and agreed to the published version of the manuscript.

6.2. Data Availability Statement

The data presented in this study are available on request from the corresponding author.

6.3. Funding

The authors received no financial support for the research, authorship, and/or publication of this article.

6.4. Conflicts of Interest

The authors declare no conflict of interest.

7. References

- [1] Toniolo, H., Parker, G., Voller, V., & Beaubouef, R. T. (2006). Depositional turbidity currents in Diapiric Minibasins on the continental slope: Experiments - Numerical simulation and upscaling. *Journal of Sedimentary Research*, 76(5–6), 798–818. doi:10.2110/jsr.2006.072.
- [2] Widyastuti, I., Thaha, M. A., Lopa, R. T., & Hatta, M. P. (2022). Dam-Break Energy of Porous Structure for Scour Countermeasure at Bridge Abutment. *Civil Engineering Journal (Iran)*, 8(12), 3939–3951. doi:10.28991/CEJ-2022-08-12-019.
- [3] Feizi, A. (2018). Hydrodynamic Study of the Flows Caused by Dam Break around Downstream Obstacles. *The Open Civil Engineering Journal*, 12(1), 225–238. doi:10.2174/1874149501812010225.
- [4] Lu, X., Peng, X., & Du, S. (2020). Research on Construct Scenario-Response Emergency Model of Dam Break. *Journal of Physics: Conference Series*, 1626, 012037. doi:10.1088/1742-6596/1626/1/012037.
- [5] Yaghoubi, S., Afshin, H., Firoozabadi, B., & Farizan, A. (2017). Experimental Investigation of the Effect of Inlet Concentration on the Behavior of Turbidity Currents in the Presence of Two Consecutive Obstacles. *Journal of Waterway, Port, Coastal, and Ocean Engineering*, 143(2), 4016018. doi:10.1061/(asce)ww.1943-5460.0000358.
- [6] Yagmur, S., Dogan, S., Aksoy, M. H., Goktepli, I., & Ozgoren, M. (2017). Comparison of flow characteristics around an equilateral triangular cylinder via PIV and Large Eddy Simulation methods. *Flow Measurement and Instrumentation*, 55(April), 23–36. doi:10.1016/j.flowmeasinst.2017.04.001.
- [7] Altinakar, S., Graf, W. H., & Hopfinger, E. J. (1990). Effet de la sedimentation sur les courants de turbidité dans un lit a faible pente. *Journal of Hydraulic Research*, 28(1), 55–80. doi:10.1080/00221689009499147.
- [8] Ali, M. S., Hasan, M. M., & Haque, M. (2017). Two-Dimensional Simulation of Flows in an Open Channel with Groin-Like Structures by iRIC Nays2DH. *Mathematical Problems in Engineering*, 2017. doi:10.1155/2017/1275498.
- [9] Ali, M. S., Hosoda, T., & Kimura, I. (2015). Development of a Nonlinear $k - \epsilon$ Model Incorporating Strain and Rotation Parameters for Prediction of Complex Turbulent Flows. *International Journal of Partial Differential Equations*, 2015, 1–15. doi:10.1155/2015/105809.
- [10] Reunsumrit, J. (2013). The lattice boltzmann method for investigating the fluid flow pattern in 2D channel through triangle obstacle. *Applied Mathematical Sciences*, 7(65–68), 3215–3223. doi:10.12988/ams.2013.34225.
- [11] Takebayashi, H., & Shimizu, Y. (2014). iRIC software Nays2DH solver manual. iRIC software, Reston, United States.
- [12] Khavasi, E., Jamshidnia, H., Firoozabadi, B., & Afshin, H. (2012). Experimental investigation of flow structure of a density current encountering a basal obstacle. *Experimental investigation of flow structure of a density current encountering a basal obstacle. Proceedings of the 8th International Symposium on Ultrasonic Doppler Methods for Fluid Mechanics and Fluid Engineering*, 1-21 September, 2012, Dresden, Germany.
- [13] Huang, Z. J., Xu, T. B., Zhu, D. Z., & Zhang, S. D. (2023). Simulation of open channel flows by an explicit incompressible mesh-free method. *Journal of Hydrodynamics*, 35(2), 287-298. doi:10.1007/s42241-023-0020-4.
- [14] Wu, Y., Wang, D., Li, P., & Niu, Z. (2023). Experimental investigation of dry granular flows down an inclined channel against a wall-like obstacle of limited width. *Acta Geotechnica*, 18(4), 2141-2154. doi:10.1007/s11440-022-01714-2.
- [15] Dissanayaka, K. D. C. R., & Tanaka, N. (2023). Scour around the single emergent cylinder due to subcritical and supercritical approach flow conditions. *ISH Journal of Hydraulic Engineering*, 1-16. doi:10.1080/09715010.2023.2212632.
- [16] Widyastuti, I., Thaha, M. A., Lopa, R. T., & Hatta, M. P. (2021). The influence of energy-reducing structure placement on friction velocity distribution in open channel. *IOP Conference Series: Earth and Environmental Science*, 841, 012019. doi:10.1088/1755-1315/841/1/012019.